*J. Zool., Lond.* (1981) **194**, 53–66

# Influence of pectoral fin shape on thrust and drag in labriform locomotion

R. W. BLAKE*

*Department of Zoology, University of Cambridge*

(*Accepted 10 June 1980*)

(With 7 figures in the text)

A simple hydromechanical model of the influence of pectoral fin geometry on thrust is developed. The model contains a shape factor (analogous to that employed by Weis-Fogh (1973) in his analysis of the influence of wing shape on normal hovering in insects and hummingbirds), which is calculated for various hypothetical fin shapes and the pectoral fins of *Pterophyllum eimekei* and *Trichogaster tricopterus*. The model predicts that fish which swim in the drag-based labriform mode are more likely to have triangular fins than square or rectangular ones, and this is generally the case.

The influence of pectoral fin shape on labriform locomotion is investigated further experimentally, using dead fish and a model Angelfish fitted with various model pectoral fin shapes (circular disc, square, rectangular or triangular fins of equivalent wetted surface area). Frictional and pressure drag determinations were made with the model fins attached to the end of a narrow spar (so that the flow around them would not influence that around the body) with the fins orientated either parallel (for frictional drag determinations) or "broadside on" (for pressure drag determinations) to the incident flow.

Values for the frictional drag of the various fin types were essentially the same for any given terminal velocity. The pressure drag of square and rectangular fins is about 14% less than that of triangular fins of the same area over a range of terminal velocities. When the fins are directly attached to the sides of the model fish and orientated "broadside on" to the flow the total drag force is higher (for any given value of the terminal velocity) than the values measured when the fins were placed, with the same orientation, on the ends of a spar. The difference is probably due to "interference drag" produced by the fins, due to the effect of the vorticity which they shed into the flow over the body.

## Contents

| | Page |
|---|---|
| Introduction | 54 |
| A simple model of the influence of pectoral fin geometry on thrust | 54 |
| An experimental investigation into pectoral fin and body drag | 55 |
| Terminal velocity experiments | 55 |
| Results of the "drop-tank" experiments on *P. eimekei* | 55 |
| "Drop-tank" experiments on model fish | 58 |
| Calibration of the plastic fish model | 58 |
| Fin shapes and settings | 58 |
| Drag components | 63 |
| Discussion | 63 |
| References | 66 |

*Present address: Department of Zoology, University of British Columbia, Vancouver, Canada.



0022–5460/81/050053 + 14 $02.00/0

## Introduction

The variety of pectoral fin shapes exhibited by teleosts which swim in the labriform (pectoral fin) modes is striking. Pectoral fin shapes range from the broad-based, truncated triangular fins of *Pterophyllum eimekei* to the narrow-based, spatulate fins of forms such as *Trichogaster tricopterus*.

In previous papers on the drag-based mechanism of labriform locomotion, a detailed model of the pectoral fin-beat cycle in the Angelfish was developed (Blake, 1979*a*, *b*, on the power stroke; in press, on the recovery stroke and overall fin-beat cycle propulsive efficiency). Here, the effects of pectoral fin shape and kinematics on the thrust produced by a rowing pectoral fin are assessed by applying a simple hydromechanical model to a series of simple geometrical shapes (each of which represents a "hypothetical pectoral fin shape") and the fins of *P. eimekei* and *T. trichopterus*. Fin shape and drag is investigated experimentally, employing dead Angelfish and a series of model Angelfish, pectoral fin shape combinations.

## A simple model of the influence of pectoral fin geometry on thrust

Confining our attention to the power stroke phase of the fin-beat cycle (see Blake 1979*a*, *b*, for a detailed account) and ignoring the forward velocity of the fish, we can write:

$$dF_n = \tfrac{1}{2}\rho(r\omega)^2 c\, dr\, C_n \tag{1}$$

$$dT = dF_n \sin\gamma = \tfrac{1}{2}\rho(r\omega)^2 c\, dr\, C_n \sin\gamma \tag{2}$$

where $dF_n$ is the normal force and $dT$ is the thrust force acting on a pectoral fin blade-element. $C_n$ is a normal force coefficient, $\rho$ is the fluid density, $\gamma$ is the positional angle of the fin, $\omega$ is the angular velocity of the fin and $c$ is its chord at $r$, the distance from the base of the fin to the midpoint of any given pectoral fin blade-element.

The impulse of the power stroke ($P_t$) can be written as:

$$P_t = \int_{r=0}^{R} \int_{t=0}^{t_p} dT\, dt$$

$$= \int_0^R \int_0^{t_p} \tfrac{1}{2}\rho(r\omega)^2 c\, dr\, C_n \sin\gamma\, dt$$

$$= \tfrac{1}{2}\rho C_n \int_0^R r^2 c\, dr \int_0^{t_p} \omega^2 \sin\gamma\, dt \tag{3}$$

where $R$ is the total length of the fin and $t_p$ is the duration time of the power stroke. Calling:

$$\int_0^R r^2 c\, dr = I_1 R^2 A \tag{4}$$

(where $A$ is the frontally projected area of the fin, $I_1$ is a numerical constant). Noting that:

$$P_b = \tfrac{1}{2}\rho V^2 S_w C_b t_o \tag{5}$$

(where $P_b$ is the impulse of the drag force acting on the body over the fin-beat cycle time ($t_o$), $S_w$ is the total wetted surface area of the body, $C_b$ is the drag coefficient of the body and $V$ its forward velocity) and:

$$P_b = 2P_t \tag{6}$$

(as there are two pectoral fins) we can write (from 3, 4, 6 and 7):

$$\tfrac{1}{2}\rho V^2 S_w C_b t_o = C_n I_1 R^2 A\rho \int_0^{t_p} \omega^2 \sin\gamma \, dt \tag{7}$$

Therefore, thrust is directly proportional to $I_1$, the value of which is dependent on fin geometry. For square and rectangular fins $I_1 = 0{\cdot}33$. This value is not affected by a change in the base to height ratio for a planform of any given area. $I_1$ for triangular planforms is 0·5, irrespective of base to height ratio (Blake, 1979*a*). Values of $I_1 = 0{\cdot}43$ and 0·38 were measured for the pectoral fins of *P. eimekei* and *T. trichopterus* respectively.

## An experimental investigation into pectoral fin and body drag

### *Terminal velocity experiments*

Dead Angelfish or Angelfish models were dropped to terminal velocity in a large tank (1·33 m high × 0·5 m wide × 0·5 m breadth) of water. The specimens were held in the jaws of an aluminium clip, with the trailing edge of the caudal fin about level with the surface of the water. The clip was spring loaded and connected to a "pulling" solenoid (mounted on a Dexion framework) which, when activated, opened the clip releasing the specimen.

As they fell specimens were filmed (64 frames $s^{-1}$, Bolex H16 reflex cinecamera, Pan F 16 mm film at f 5·6 or f 8) against a grid (2·5 cm squares) which was placed at the back of the tank. The cinecamera (mounted on a Dexion framework) was set at a horizontal level (a small spirit level was attached to the top surface of the camera) in the region where it was thought that the specimen would attain its terminal velocity. Before an experiment the camera was inclined upward at an angle of 20° from the horizontal. During the course of an experiment the operator would "pan down" the camera through an angle (measured by a goniometer attached to the upper surface of the camera) of about 40°.

A length of thread was stretched across the top of the tank, directly above the specimen. A person assisting in the experiment could use this as a sight and stop the experiment if the specimen moved forwards or backwards during its descent. The camera operator would stop the experiment if the specimen fell to the left or right.

Processed films were analysed frame by frame on an analytical projector (Vanguard Instrument Corporation Motion Analyser), a note was made of any "flutter" or tendency to depart from a straight downward course, such sequences were not analysed further. Most specimens reached terminal velocity at a level of ± 5° of the optical axis of the camera, giving a minimum of image distortion.

Specimens were loaded with small lead pellets in order to change their buoyancy. Animals or models which did not fall steadily (due to body or fin curvature) during "trial runs" were stiffened with fine steel wire.

### *Results of the "drop-tank" experiments on* ***P. eimekei***

The frictional drag coefficient of a smooth flat plate or a streamlined body, orientated parallel to the direction of the flow can be calculated from an empirical equation derived

TABLE I

*Data on a specimen of* ***P. eimekei*** *falling to terminal velocity with both pectoral fins in the "open" position* (A) *and after the fins had been amputated* (B)

| (A) $L$ = 8·0 cm, $S_{(tot)}$ = 48·2 cm² | | | | (B) $L$ = 8·0 cm, $S_w$ = 44·0 cm² | | | |
|---|---|---|---|---|---|---|---|
| $\bar{V}_t$(cm s$^{-1}$) | $\bar{C}_{b(exp)}$ | $\bar{C}_{b(the)}$ | $\frac{\bar{C}_{b(exp)}}{\bar{C}_{b(the)}}$ | $\bar{V}_t$(cm s$^{-1}$) | $\bar{C}_{b(exp)}$ | $\bar{C}_{b(the)}$ | $\frac{\bar{C}_{b(exp)}}{\bar{C}_{b(the)}}$ |
| 1·48 | 0·132 | 0·039 | 3·38 | 1·43 | 0·038 | 0·039 | 0·97 |
| 2·81 | 0·13 | 0·028 | 4·64 | 2·0 | 0·037 | 0·033 | 1·11 |
| 3·26 | 0·10 | 0·026 | 3·85 | 2·11 | 0·038 | 0·032 | 1·19 |
| 3·38 | 0·096 | 0·026 | 3·69 | 2·23 | 0·035 | 0·031 | 1·14 |
| 3·94 | 0·088 | 0·024 | 3·67 | 2·49 | 0·031 | 0·030 | 1·05 |
| 4·10 | 0·086 | 0·023 | 3·74 | 2·62 | 0·030 | 0·029 | 1·03 |
| 4·36 | 0·085 | 0·022 | 3·86 | 2·93 | 0·029 | 0·027 | 1·07 |
| 4·52 | 0·085 | 0·022 | 3·86 | 3·12 | 0·029 | 0·027 | 1·07 |
| 4·91 | 0·084 | 0·021 | 4·00 | 3·28 | 0·030 | 0·026 | 1·15 |
| 5·12 | 0·080 | 0·02 | 4·00 | 3·51 | 0·028 | 0·025 | 1·11 |
| 5·34 | 0·079 | 0·02 | 3·95 | 3·67 | 0·029 | 0·024 | 1·21 |
| 5·57 | 0·078 | 0·02 | 3·90 | 3·83 | 0·029 | 0·024 | 1·21 |
| 5·81 | 0·075 | 0·02 | 3·75 | 3·89 | 0·025 | 0·024 | 1·04 |
| 6·02 | 0·074 | 0·019 | 3·89 | 3·92 | 0·024 | 0·024 | 1·00 |
| 6·32 | 0·074 | 0·019 | 3·89 | 4·06 | 0·026 | 0·023 | 1·14 |
| 6·71 | 0·066 | 0·018 | 3·67 | 4·18 | 0·024 | 0·023 | 1·04 |
| 6·92 | 0·063 | 0·018 | 3·50 | 4·23 | 0·022 | 0·023 | 0·97 |
| 7·03 | 0·061 | 0·018 | 3·39 | 4·58 | 0·022 | 0·023 | 0·97 |
| 7·26 | 0·060 | 0·017 | 3·53 | 4·66 | 0·026 | 0·022 | 1·19 |
| 7·38 | 0·059 | 0·017 | 3·47 | 5·08 | 0·021 | 0·021 | 1·00 |
| 7·92 | 0·055 | 0·017 | 3·24 | 5·13 | 0·018 | 0·021 | 0·87 |
| 8·13 | 0·053 | 0·017 | 3·12 | 5·27 | 0·018 | 0·021 | 0·87 |
| 8·29 | 0·051 | 0·016 | 3·19 | 5·51 | 0·020 | 0·020 | 1·00 |
| 8·63 | 0·048 | 0·016 | 3·00 | 5·67 | 0·019 | 0·020 | 0·95 |
| 8·72 | 0·048 | 0·016 | 3·00 | 5·90 | 0·020 | 0·019 | 1·05 |
| | | | | 5·97 | 0·019 | 0·019 | 1·00 |
| | | | | 6·05 | 0·019 | 0·019 | 1·00 |
| | | | | 6·16 | 0·020 | 0·019 | 1·05 |
| | | | | 6·38 | 0·020 | 0·019 | 1·05 |
| | | | | 6·51 | 0·202 | 0·018 | 1·11 |
| | | | | 6·90 | 0·019 | 0·018 | 1·06 |
| | | | | 7·16 | 0·019 | 0·018 | 1·06 |
| | | | | 7·28 | 0·019 | 0·017 | 1·11 |
| | | | | 7·48 | 0·019 | 0·017 | 1·11 |
| | | | | 7·59 | 0·019 | 0·017 | 1·11 |
| | | | | 7·92 | 0·020 | 0·017 | 1·18 |
| | | | | 8·16 | 0·019 | 0·016 | 1·19 |
| | | | | 8·51 | 0·017 | 0·016 | 1·06 |
| | | | | 8·69 | 0·019 | 0·016 | 1·06 |
| | | | | 9·34 | 0·020 | 0·015 | 1·33 |
| | | | | 9·81 | 0·019 | 0·015 | 1·26 |
| | | | | 9·92 | 0·019 | 0·015 | 1·26 |
| | | | | 10·51 | 0·017 | 0·014 | 1·21 |
| | | | | 10·87 | 0·017 | 0·014 | 1·21 |

Notation: $\bar{V}_t$ = the mean value of the terminal velocity for $n$ determinations (usually from 5–10 determinations, the range of terminal velocity values recorded rarely exceeded 3% of the mean value for experiments types A and B).

by Blasius. The value of the frictional drag coefficient can be considered as an estimate of the theoretically possible minimum drag force acting on the fish

$$C_{b(the)} = 1{\cdot}33\,(R_b^{-0{\cdot}5}) \tag{8}$$

where $C_{b(the)}$ is the frictional drag coefficient of the body and $R_b$ is the Reynolds Number ( $= LV/\upsilon$, where $\upsilon$ is the kinematic viscosity of the fluid).

Mean values of $C_{b(the)}$ at a range of terminal velocities are compared with the experimentally determined values of the drag coefficient of the body ($C_{b(exp)}$) in Table I for a specimen of *P. eimekei*, dropped to terminal velocity with its pectoral fins "open" (in a position typical of the power stroke phase of the fin-beat cycle) and for the same fish after the pectoral fins had been amputated. The experimentally determined values of the drag coefficients of the body at the given values of $R_b$.

Table I shows that:

(1) When the pectoral fins are amputated and the specimens dropped to terminal velocity, values of $\bar{C}_{b(exp)}$ are about 10% higher than the calculated values of $\bar{C}_{b(the)}$ $\overline{(\bar{C}_{b(exp)}/\bar{C}_{b(the)})} = 1{\cdot}09$, $N = 44$, s.d. $= 0{\cdot}10$, for a range of $R_b$ of 1144–8696).

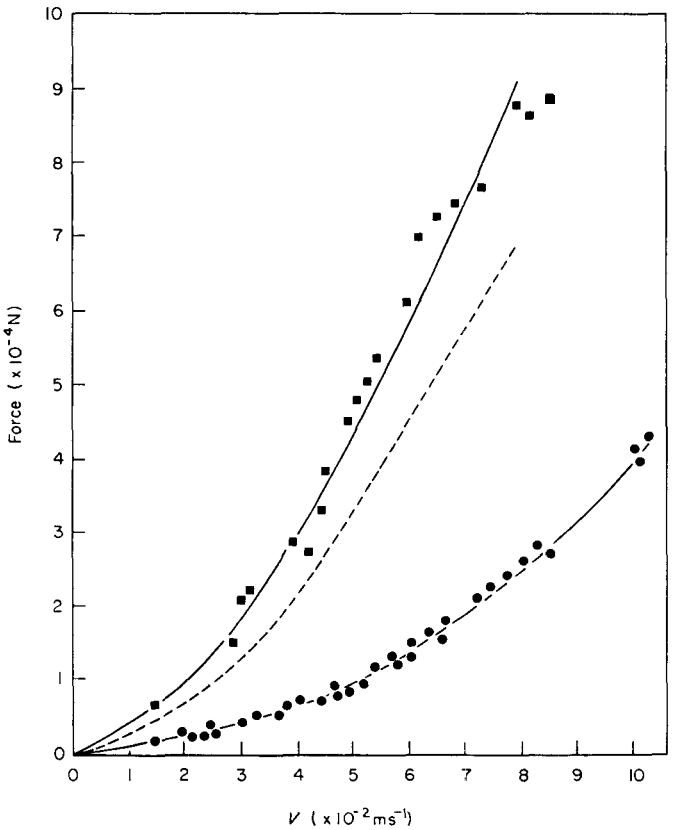


FIG. 1. The drag force acting on a specimen of *P. eimekei* (Length = 8·05 cm) with its pectoral fins in the "open" position (■) and with no pectoral fins (●) is plotted against velocity. The broken line indicates the difference (due to pressure and interference drag) between the two experimentally obtained curves.

(2) With the pectoral fins in the "open" position the mean value of the experimentally determined drag coefficients exceeds the calculated friction drag values by a factor of 3·65 ($\overline{C_{b(exp)}/C_{b(the)}}$) = 3·65, $N$ = 25, s.d. = 0·37, $R_b$ range: 1184–6796).

Values of the drag force acting on the animal are plotted against velocity for fish with their pectoral fins in the "open" position and for animals without pectoral fins in Fig. 1.

### *"Drop-tank" experiments on model fish*

A model fish (based on the planform of a specimen of *P. eimekei*: length = 14·3 cm) was made in Perspex (approximately 3 mm thick). The model was weighted by lead pellets at the nose. A Perspex spar (6·0 cm in length, 1·5 mm thick), to which model fins (approximately 1·5 mm thick) could be attached, could be passed through the model (at 90 to the plane of the median, longitudinal axis of the model) at a point corresponding to the position of the pectoral fins in the real fish on which the model was based. The spar could be rotated through 180°.

#### *Calibration of the plastic fish model*

The model was dropped over a range of terminal velocities without any appendages. On average the values of $\bar{C}_{b(exp)}$ are about 19% higher than those of $\bar{C}_{b(the)}$($\overline{(\bar{C}_{b(exp)}/\bar{C}_{b(the)})}$ = 1·19, $N$ = 15, s.d. = 0·06, $R_b$ range: 2814–16,286. (See Blake, 1979*a*, Table 8 for raw data and a statistical analysis).

The model was fitted with the spar and dropped again. The value of $\overline{(\bar{C}_{b(exp)}/\bar{C}_{b(the)})}$ increased to 1·44 ($N$ = 20, s.d. = 0·10, $R_b$ range: 3248–14,694. (Further details are given in Blake, 1979*a*, Table 9).

#### *Fin shapes and settings*

The model fish was dropped to terminal velocity, fitted with either circular, square, rectangular (narrow based or broad based mounted with the long axis spanwise), or

TABLE II

*Summary of the data gained from the model fish, fin shape combination terminal velocity experiments. All notation is defined in the text*

| Fin shape | Dimensions (cm) | Fin setting | $N$ | $\bar{C}_{b(exp)}/\bar{C}_{b(the)}$ | s.d. | $R_{b(range)}$ |
|---|---|---|---|---|---|---|
| Circular disc | 2·7* | A | 23 | 1·48 | 0·13 | 3094–15,210 |
| Square | 2·92×2·92 | A | 15 | 1·49 | 0·09 | 2702–15,200 |
| | | B | 13 | 5·84 | 0·02 | 3660–13,874 |
| | | C | 15 | 7·54 | 0·34 | 3612–14,756 |
| Rectangular | 1·94×4·38 | A | 12 | 1·51 | 0·05 | 3738–14·238 |
| | | B | 12 | 5·57 | 0·15 | 3822–14,476 |
| | | C | 11 | 6·84 | 0·27 | 4102–14,028 |
| Rectangular | 1·46×5·84 | A | 22 | 1·53 | 0·06 | 2828–14,182 |
| | | B | 10 | 5·44 | 0·22 | 3892–14,336 |
| | | C | 10 | 7·09 | 0·34 | 4102–13,034 |
| Triangular | 5·1×3·34** | A | 14 | 1·57 | 0·06 | 3374–14,672 |
| | | B | 10 | 5·12 | 0·17 | 4018–13,972 |
| | | C | 11 | 5·87 | 0·23 | 2898–13,696 |

*Refers to radius; **Refers to base×height.

triangular (mounted with the apex pointing towards the body) plastic fins. All of the model fins had the same surface area (total wetted area = 17·0 cm², frontally projected area = 8·5 cm²). The dimensions of the fins are given in Table II.

Three types of experiment were performed on each of the model fish and pectoral fin shape combinations:

Type A: The fins were placed on the ends of the spar and adjusted so that they would be parallel to the flow.

Type B: The fins were placed on the ends of the spar and adjusted so that they would be "broadside on" to the flow.

Type C: The fins were placed directly on to the model and adjusted so that they would be "broadside on" to the flow.

Raw data and a statistical analysis of the terminal velocity experiments for the various model fish and plastic fin shape combinations are given in Blake, 1979*a* (Tables: 10–14, 15–18 and 19–22 for experiments type A, B, and C respectively). The information is summarized in Table II of this paper, which shows that:

1. Values of $\overline{(C_{b(exp)}/C_{b(the)})}$ for experiment type A < B < C for square (C is ×1·29B and ×5·06A; B is 3·29A), rectangular (for base : height, 1·00 : 2·26; C is ×1·23B and

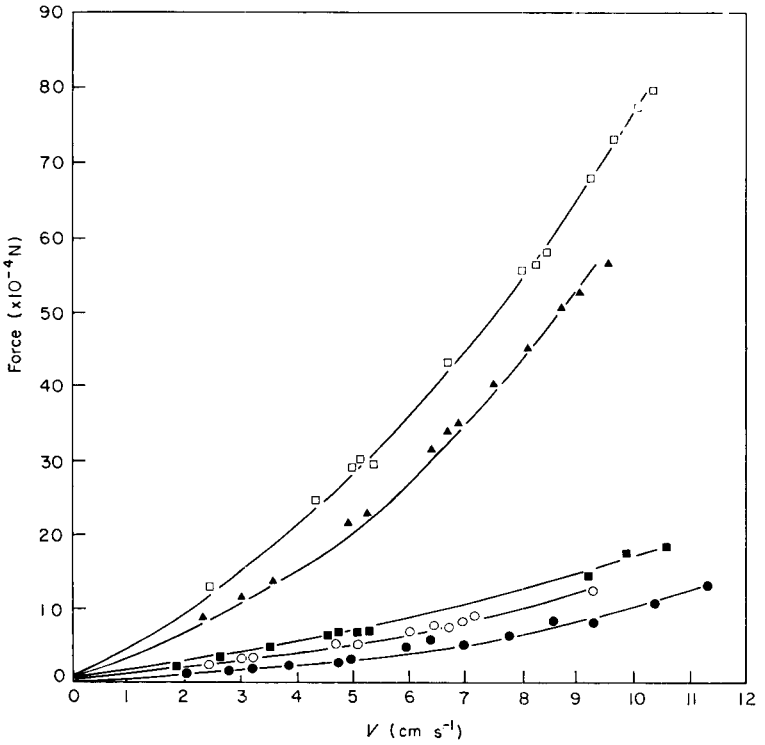


FIG. 2. The drag force acting on the model fish is plotted against velocity for the case of no appendages (●), the body and spar (○), the body, spar and square fins, orientated parallel to the flow (■), the body, spar and square fins orientated "broadside on" to the flow (▲) and the body and square fins attached directly on to the sides of the body and orientated "broadside on" to the flow (□).

$\times$4·53A, B is $\times$3·67A. For base : height, 1·00 : 4·00; C is $\times$1·30B and 4·63A, B is 3·26A) fin shapes.

2. The value of $\overline{(\bar{C}_{b(exp)}/\bar{C}_{b(the)})}$ for experiment type A for a circular disc is < square < rectangle (base : height, 1·00 : 2·26) < rectangle (base : height, 1·00 : 4·00) < triangle. For experiment type B the value of the triangle is < rectangle (base : height, 1·00 : 4·00) < rectangle (base : height, 1·00 : 2·26) < square. For experiment type C the value of the triangle is < rectangle (base : height, 1·00 : 2·26) < rectangle (base : height, 1·00 : 4·00) < square.
3. The percentage differences between the minimum and maximum values of $\overline{(\bar{C}_{b(exp)}/\bar{C}_{b(the)})}$ are 6% (between the circular disc and the triangle), 14·1% (between the triangle and square) and 28·5% (between the triangle and square) for experiment types A, B and C respectively.

The experimentally determined drag force acting on the model for experiment types A, B and C is plotted against velocity in Fig. 2 (for square fins), Fig. 3 (for rectangular fins) and Fig. 4 (for triangular fins).

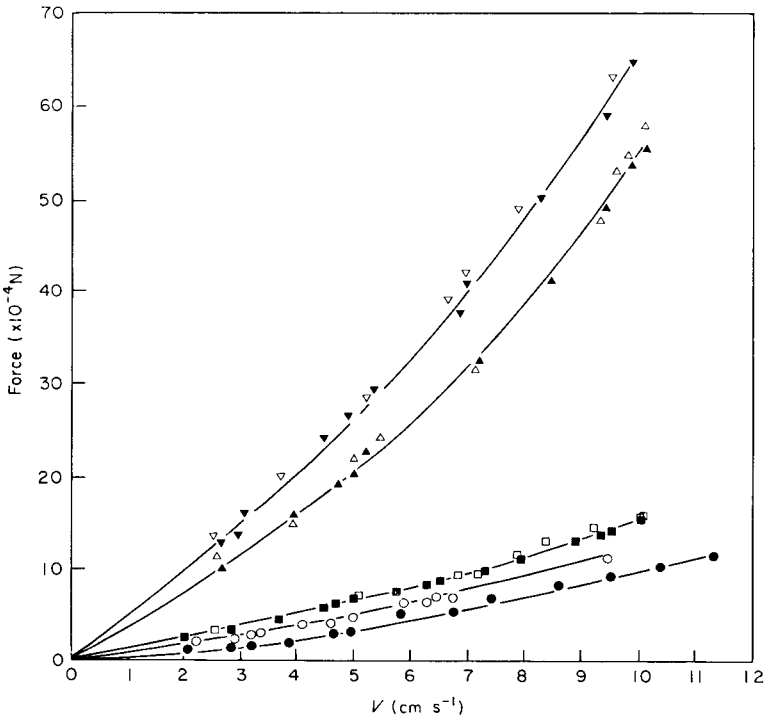


FIG. 3. The drag force acting on the fish model is plotted against velocity for the case of no appendages (●), the body and spar (○), the body, spar and rectangular fins ((□), for height : base, of 1·00 : 2·26; (■) for height : base of 1·00 : 4·00) orientated parallel to the flow. The body, spar and rectangular fins ((△), for height : base, of 1·00 : 2·26; (▲) for height : base of 1·00 : 4·00) orientated "broadside on" to the flow and the body and rectangular fins ((□), for height : base, of 1·00 : 2·26; (○) for height : base, of 1·00 : 4·00) attached directly on to the sides of the body and orientated "broadside on" to the flow.

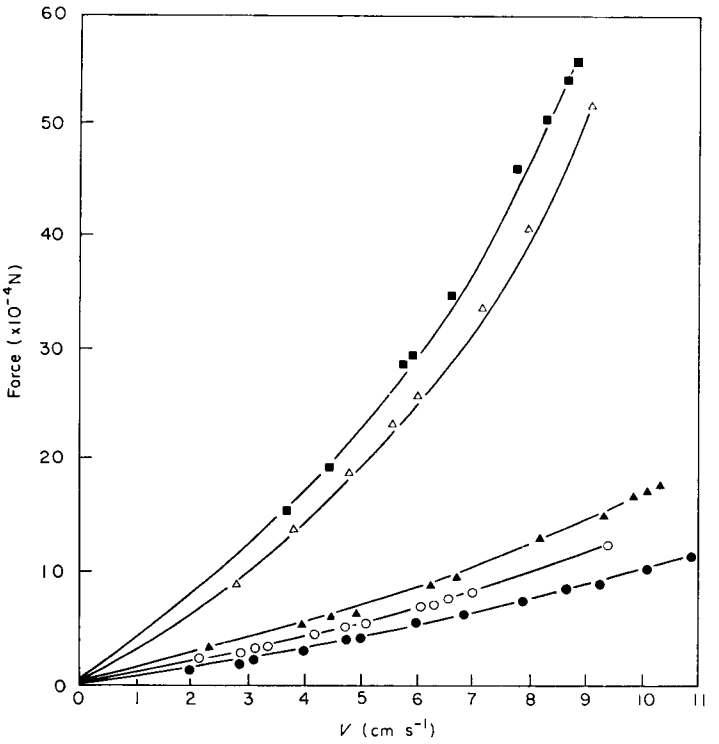


FIG. 4. The drag force acting on the model fish is plotted against velocity for the case of no appendages (●), the body and spar (○), the body, spar, and triangular fins orientated parallel to the flow (▲), the body, spar, and triangular fins orientated "broadside on" to the flow (△) and the body and triangular fins attached directly to the body (■) and orientated "broadside on" to the flow.

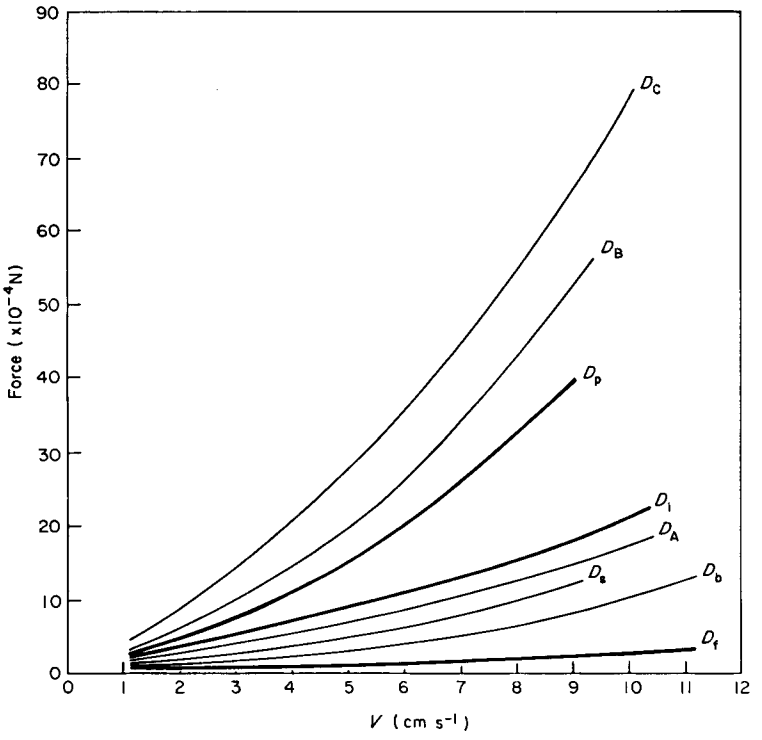


FIG. 5. Drag forces acting on the model fish when fitted with square fins. All notation is defined in the text.

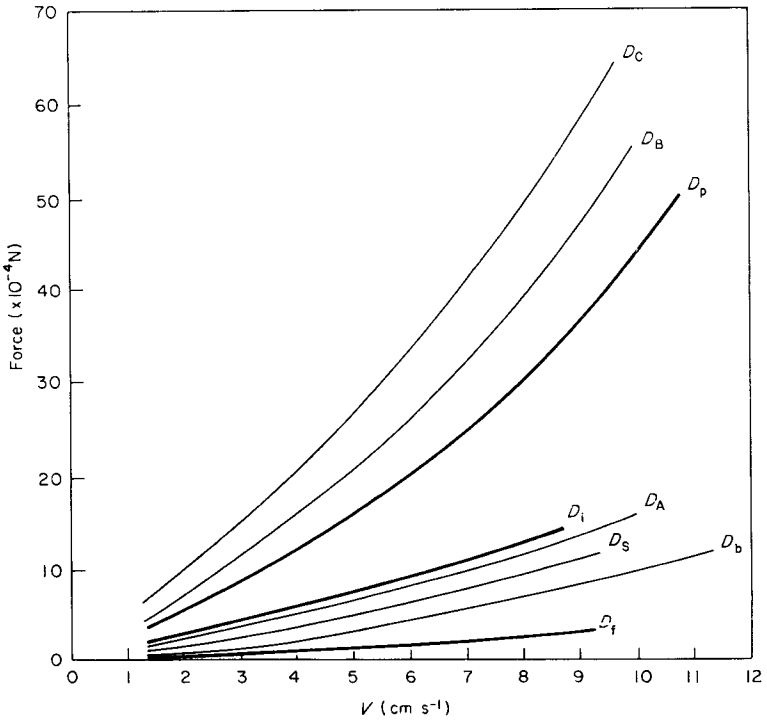


FIG. 6. Drag forces acting on the model fish when fitted with rectangular fins. All notation is defined in the text.

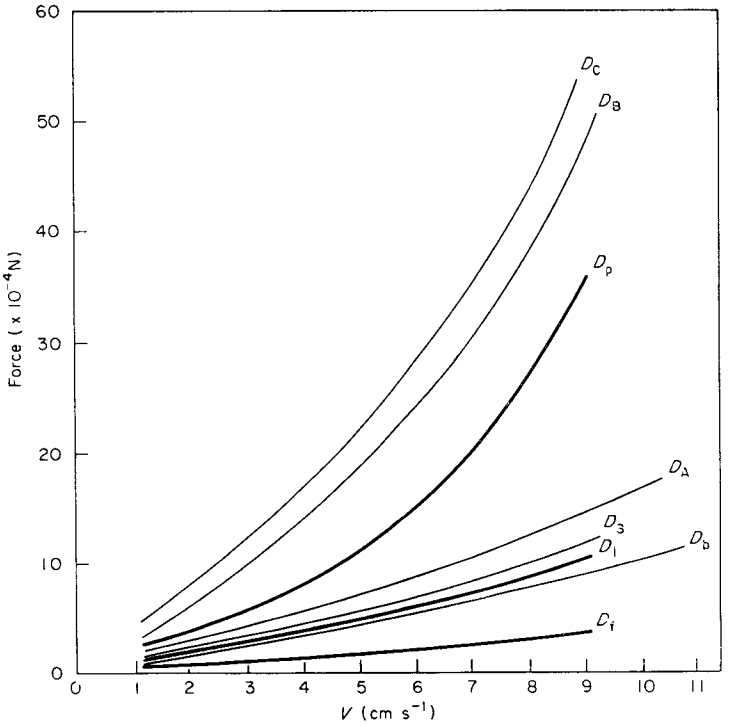


FIG. 7. Drag forces acting on the model fish when fitted with triangular fins. All notation is defined in the text.

*Drag components*

The force versus velocity curves obtained from the "drop-tank" experiments are re-plotted in Figs 5, 6 and 7 (for square, rectangular and triangular fins respectively), for experiments the A ($D_A$), B ($D_B$) and C ($D_C$). The drag force acting on the body ($D_b$) and on the body plus spar ($D_s$) are also plotted.

The friction drag ($D_f$, acting on the fins when they are orientated parallel to the incident flow) and pressure drag ($D_p$, acting when the fins are orientated "broadside on" to the flow) are given by:

$$D_f = D_A - D_s \tag{9}$$

$$D_p = D_B - D_s \tag{10}$$

and are plotted on Figs 5, 6 and 7 for square, rectangular and triangular fins respectively.

We can recognize another drag component, which arises due to the interference between the flow around the fins and the body. The interference drag is given by:

$$D_i = D_C - (D_b + D_p) \tag{11}$$

and is also plotted on Figs 5–7, which show that:

1. The value of $D_f$ is virtually the same for square, rectangular and triangular fins at all values of $V$.
2. Values of $D_p$ are similar for square and rectangular fins at all values of $V$. Values of $D_p$ for triangular fins are lower than those for square or rectangular fins at velocities greater than about 6·0 cm $s^{-1}$.
3. Interference drag for the square fins is about twice that of the triangular fins at all values of $V$.

During swimming, the pectoral fins of the Angelfish move backwards relative to its body. In the "drop-tank" experiments on dead Angelfish and model fish however, the fins were fixed in position. Blake (1979*a*, *b*) has shown that the relative velocities of the proximal half of the Angelfish pectoral fin (where interference drag is generated) in forward swimming are low. It is assumed, therefore, that the two situations are fluid dynamically comparable.

## Discussion

The simple model of the influence of fin geometry on thrust production indicates that fish which swim in the drag-based labriform mode are more likely to have triangular fins ($I_1$ = 0·5) than square or rectangular ones ($I_1$ = 0·33) and this is generally the case.

The pectoral fins of *P. eimekei* ($I_1$ = 0·43) have the planform of a truncated triangle, giving a value of $I_1$ less than 0·5. The broad base of the fins however, facilitates a great independence of motion of individual fin-rays, permitting complicated waveforms to be passed down the pectoral fins. During hovering up to three-quarters of a wavelength may be present on a pectoral fin at any instant. The pectoral fins of *T. trichopterus* are narrow based and rarely exhibit as much as one quarter of a wavelength during hovering. Hovering in *T. trichopterus* is effected primarily by the "bodily" movement of the pectoral fins. The value of $I_1$ (0·38) for the pectoral fins of *T. trichopterus* is less than that of *P. eimekei*, as the spatulate form of the fins reduces their chord distally.

It is interesting to note that the value of $I_1$ does not change as the ratio of the minor to

major axis of a rectangular planform or the height to base ratio of a triangular planform of a given area is changed. The basic pectoral fin shapes evolved by teleosts which swim in the labriform modes (largely triangular and wedge shapes), probably reflect the results of intense selection pressure for hydromechanical efficiency. However, the variations on the principal planforms (so useful to the taxonomist), are probably not of any great hydromechanical significance.

Weis-Fogh (1973) considers the influence of wing shape on the normal hovering (body is held vertically and the wings beat in a horizontal plane) of insects and hummingbirds. Using a blade–element analysis he calculated the average lift of the wings, required to support an insect of given weight, with wings of a given shape and size, geometry of wing stroke and wing beat frequency.

Weis-Fogh calculated the average lift of the wings ($\bar{L}$) from:

$$\bar{L} = \tfrac{1}{2}\rho\pi^2 n^2 \phi^2 \bar{C}_L \int_{r=0}^{r=R} c(r) r^2 \, dr \int_{t=0}^{t=\frac{1}{n}t} \cos^2(2\pi n t) \, dt$$

(Weis-Fogh, 1973, equation 8) where n is the wing beat frequency, $\phi$ is the angle swept by a wing, $r$ is the distance along the wing (total length $R$) from its base, $c$ is the wing chord and $C_L$ is an average lift coefficient for the wing. The first term in the equation can be treated as a constant and the third term is simply a function of time. The second term is the integral of the derivative with respect to $r$ of the second moment of the wing area and is analogous to the term on the left hand side of equation 4 of this paper. Weis-Fogh gives a general expression for the second moment of wing area ($S$): $S = \sigma c R^3$ (Weis-Fogh, 1973, equation 7), where $\sigma$ is a shape factor. The shape factor is equivalent to $I_1$.

Weis-Fogh simplified his analysis by approximating the forms of the wings of many insects to a semi-ellipse ($\sigma = 0{\cdot}39$). He justified the simplification by pointing out that a semi-ellipse "fits" the outer two-thirds of the wings well and it is that part of the wings which produce most of the lift force. The same simplification and justification could be applied to fish which swim in the labriform mode and possess spatulate fins (e.g. the value of $I_1$ for *T. trichopterus* (0·38) is within 3% of the shape factor of the semi-ellipse).

To my knowledge there are only four published studies in which the drag of a swimming fish has been indirectly estimated from dead-drag, free-fall terminal velocity experiments. Unfortunately, two of the studies (Magnan & St. Laque, 1929; Magnan, 1931) do not contain sufficient data for the calculation of the drag coefficients and the Reynolds Numbers at which the fish reached terminal velocity. Information on the other two studies (Richardson, 1936; on *Scomber scomber* and *Clupea herengus* and Gero, 1952; on *Amia calva*) is summarized by Webb (Webb, 1975, Table 5).

Values of the drag coefficients calculated by Richardson and by Gero are about two orders of magnitude higher than the values calculated from the standard hydrodynamic equations of resistance. Webb (1975) suggests that the fish involved in Richardson's and Gero's experiments were not allowed to reach terminal velocity, leading to an overestimation of the values of the drag coefficients. It is also possible that body and fin flutter increased the drag force acting on the fish, thereby decreasing the terminal velocity and leading to an overestimation of the drag coefficient.

Care was taken in this study to ensure that fish reached their true terminal velocity and that no serious body or fin flutter was observed. In *P. eimekei* the body is short relative to

its depth and the vertebral column is well developed and rather inflexible. Animals were often stiffened further with wire in the experiments. The pelvic, dorsal and anal fins of *P. eimekei* are short and have stiff spines at their leading edge.

Experimental determinations of the dead drag of a rigid fish or fish model, whatever the method employed (e.g. free-fall, towing, deceleration in glide, water tunnel measurements; see Webb, 1975 for a general discussion of dead drag determination methods) are only likely to lead to good estimation of the drag force acting on a swimming fish if it can be assumed that the flow pattern around a fish or fish model during a dead drag determination is similar to that general by the swimming movements of the fish. For fish which swim in the anguilliform and sub-carangiform modes (see Webb, 1975 for definitions) this is unlikely, as:

1. Experimental evidence shows that the pressure drag of a swimming fish is greater than that of the equivalent, stretched straight body (e.g. Allen, 1961, has shown that the eyes and nares of fish swimming in the carangiform mode act as roughness elements and cause boundary layer separation in some cases. Allen (1961), Walters (1962) and Freadman (in press) have shown that gill effluent can also cause boundary layer separation).
2. Friction drag is also likely to exceed the values determined for the rigid fish or fish model, due to boundary layer thinning over those regions of the body which produce the propulsive movements (Bone in Lighthill, 1971).

Fish which swim in the labriform mode will not be subject to these additional pressure and friction drag terms associated with repeated bodily flexure.

The specimen of *P. eimekei* employed in the drop-tank experiments reached terminal velocity at values of $R_b$ ranging from about $10^3$ to about $10^4$. The body of the fish can be likened to that of a smooth, rigid streamlined form and flow in the boundary layer over the animal should have been laminar. With the pectoral fins absent, values of $\bar{C}_{b(exp)}$ are of the order of 0·02 and are only about 10% greater than the calculated, theoretical minimum values given by equation 8. The difference between the calculated and experimentally determined values is probably due to small amounts of pressure drag produced by the animal.

Values of the drag coefficient of the animal's body when the pectoral fins are in the "open position", are about three and one half times greater than those found in the absence of the pectoral fins. The pressure drag produced by the fins will acount for a substantial proportion of the difference. However, the fins will influence the flow over the body and produce a certain amount of interference drag (see Blake, 1979*b*, for a discussion of the mechanism involved).

On average, values of $\bar{C}_{b(the)}$ for the model fish are about 19% greater than the calculated minimum values of the frictional drag acting on the body over a range of velocities. The difference can be attributed to pressure drag produced at the trailing edges of the model. Addition of the spar causes an increase in the value of $\overline{(\bar{C}_{b(exp)}/\bar{C}_{b(exp)})}$ due to extra frictional, and possibly small amounts of pressure and interference drag.

As expected, values of $D_r$ (Figs 5–7) were essentially the same for all of the fin shapes examined and values of $\overline{(\bar{C}_{b(exp)}/\bar{C}_{b(the)})}$ for experiment type A were less than those for type B for any given fin shape. However, it is interesting to note that the value of $\overline{(\bar{C}_{b(exp)}/\bar{C}_{b(the)})}$ for square fins is about 14% greater than that of triangular fins.

One might predict that repeating experiment type B, without the spar (experiment type C) would result in a slightly lower value of the overall drag force, due to the loss of some friction drag. However, values for experiment type B are less than those for type C for all of the fin shapes examined (Figs 5–7). The difference is probably due to interference drag, which is produced in experiment type C and not in experiment type B, as the fins are not situated sufficiently close to the body for the flow around them to affect that over the body. Triangular fins create less interference drag than square or rectangular fins, as their chord is relatively small in the region where the pressure drag they produce interacts with the flow over the body.

I am grateful to Dr K. E. Machin, Professor Sir James Lighthill and Dr C. P. Ellington for their constructive comments on this work. I would also like to thank Mr G. G. Runnalls for his technical assistance and the N.E.R.C. for financial support.

## REFERENCES

Allen, W. H. (1961). Underwater flow visualization techniques. *Tech. Publs U.S. Navy Ordn. Test Stn* No. 2759: 1–28.

Blake, R. W. (1979*a*). *The mechanics of labriform locomotion.* Unpublished Ph.D. Thesis. University of Cambridge.

Blake, R. W. (1979*b*). The mechanics of labriform locomotion I. Labriform locomotion in the Angelfish (*Pterophyllum eimekei*): an analysis of the power stroke. *J. exp. Biol.* **82:** 255–271.

Blake, R. W. (1980). The mechanics of labriform locomotion in the Angelfish II. An analysis of the recovery stroke and overall fin-beat propulsive cycle efficiency. *J. exp. Biol.* **85:** 337–342.

Freadman, M. A. (In press). Swimming energetics of striped bass (*Morone saxatilis*) and bluefish (*Pomatomus saltatrix*) II. Hydrodynamic correlates of locomotion and gill ventilation. *J. exp. Biol.*

Gero, D. R. (1952). The hydrodynamic aspects of fish locomotion. *Am. Mus. Novit.* No. 1601: 1–32.

Lighthill, M. J. (1971). Large-amplitude elongated-body theory of fish locomotion. *Proc. R. Soc. Lond.* (B) **179:** 125–138.

Magnan, A. (1931). Les caractéristiques géométriques et physiques des poissons. *Annls Sci. nat.* (10) **13:** 355–489.

Magnan, A. & St. Laque, A. (1929). Essai de theorie du poisson. *Bull. Tech. Serv. Aerotech. Paris* **50:** 1–180.

Richardson, E. G. (1936). The physical aspects of fish locomotion. *J. exp. Biol.* **13:** 63–74.

Walters, V. (1962). Body form and swimming performance in scombroid fishes. *Am. Zool.* **2:** 143–149.

Webb, P. W. (1975). Hydrodynamics and energetics of fish propulsion. *Bull. Fish. Res. Bd Can.* **190:** 1–159.

Weis-Fogh, T. (1973). Quick estimates of flight fitness in hovering animals, including novel mechanisms for lift production. *J. exp. Biol.* **59:** 169–230.